Development 137, 3315-3325 (2010) doi:10.1242/dev.055293

SPAT-1/Bora acts with Polo-like kinase 1 to regulate PAR polarity and cell cycle progression

Anna Noatynska*, Costanza Panbianco* and Monica Gotta†

SUMMARY

During asymmetric cell division, cell polarity and cell cycle progression are tightly coordinated, yet mechanisms controlling both these events are poorly understood. Here we show that the Bora homologue SPAT-1 regulates both PAR polarity and cell cycle progression in *C. elegans* embryos. We find that, similarly to mammalian cells, SPAT-1 acts with PLK-1 and not with the mitotic kinase Aurora A (AIR-1), as shown in *Drosophila*. SPAT-1 binds to PLK-1, and depletion of SPAT-1 or PLK-1 leads to similar cell division defects in early embryos, which differ from the defects caused by depletion of AIR-1. Additionally, SPAT-1 and PLK-1 depletion causes impaired polarity with abnormal length of the anterior and posterior PAR domains, and partial *plk-1*(*RNAi*) or *spat-1*(*RNAi*), but not *air-1*(*RNAi*), can rescue the lethality of a *par-2* mutant. SPAT-1 is enriched in posterior cells, and this enrichment depends on PAR polarity and PLK-1. Taken together, our data suggest a model in which SPAT-1 promotes the activity of PLK-1 to regulate both cell polarity and cell cycle timing during asymmetric cell division, providing a link between these two processes.

KEY WORDS: Cell polarity, Cell cycle, Asymmetric cell division, Polo-like kinase 1, Aurora A, PAR polarity, *C. elegans*

INTRODUCTION

Asymmetric cell division is a fundamental process for generating cell diversity (Gonczy, 2008). In addition to the spatiotemporal coordination of spindle assembly, chromosome segregation and cytokinesis, in asymmetrically dividing cells cell cycle progression is also coupled with cell polarity. Yet, how exactly these two processes are coordinated is not understood.

The *C. elegans* one-cell embryo is a powerful model in which to study cell polarity and cell cycle progression during asymmetric cell division. The first division of the embryo is asymmetric, giving origin to a larger anterior cell AB, and a smaller posterior cell P1. Cell division at the two-cell stage is asynchronous with AB dividing approximately 2 minutes before P1 (Gonczy and Rose, 2005). These asymmetries and establishment of the anteroposterior (A-P) axis of polarity depend on the conserved PAR proteins. The PDZ-containing proteins PAR-3 and PAR-6 and the atypical protein kinase PKC-3 form a complex that is enriched at the anterior cortex (Etemad-Moghadam et al., 1995; Hung and Kemphues, 1999; Tabuse et al., 1998; Li et al., 2010), whereas PAR-2, a ring-finger protein, and PAR-1, a serine-threonine kinase, are enriched at the posterior cortex of the embryo (Boyd et al., 1996; Guo and Kemphues, 1995). Anterior and posterior PAR domains are mutually exclusive (Boyd et al., 1996; Cuenca et al., 2003; Etemad-Moghadam et al., 1995; Hao et al., 2006). PAR proteins regulate asymmetric localisation of cytoplasmic proteins that specify the fate of the daughter cells and spindle positioning (Gonczy and Rose, 2005). Furthermore, PAR proteins control asynchronous mitotic entry of AB and P1, in part by promoting enrichment in AB of a positive regulator of mitotic entry, polo-like kinase 1 (PLK-1) (Budirahardja and Gonczy, 2008; Rivers et al., 2008).

We have identified *spat-1* (suppressor of *par-2*) in a screen for suppressors of the lethality of a *par-2* temperature-sensitive mutant [*par-2*(*it5ts*)] (Labbe et al., 2006). In *par-2*(*it5ts*) embryos, PAR-3, PAR-6 and PKC-3 spread to the posterior, resulting in polarity defects and lethality. Reducing the levels or the activity of the anterior PAR complex can restore the viability of *par-2*(*it5ts*) (Labbe et al., 2006; Watts et al., 1996). *spat-1* is the homologue of *bora*, a gene identified in *Drosophila* in a screen for mutations affecting asymmetric cell division of sensory cells (Hutterer et al., 2006). *Drosophila* Bora controls asymmetric cell division and centrosome maturation by binding and activating Aurora A (Hutterer et al., 2006). By contrast, human Bora promotes mitotic entry by binding to Polo-like kinase 1 (Plk1). This interaction allows phosphorylation of Plk1 by Aurora A, triggering Plk1 activation and mitotic entry (Chan et al., 2008; Macurek et al., 2008; Seki et al., 2008a; Seki et al., 2008b).

To investigate SPAT-1/Bora function in cell polarity and cell cycle progression, we took advantage of the *C. elegans* embryo, in which these two processes take place in a coordinated manner. We show that SPAT-1 binds to PLK-1 in vivo, and that depletion of either PLK-1 or SPAT-1 results in similar cell division defects that differ from those associated with Aurora A (AIR-1). SPAT-1 is enriched in posterior cells in early embryos, and this enrichment depends on PAR proteins and PLK-1. Conversely, depletion of PLK-1 or SPAT-1 results in defects in the localisation of PAR proteins. Our data suggest a model in which SPAT-1 is required for the activity of PLK-1, and not AIR-1, and both SPAT-1 and PLK-1 regulate polarity and cell cycle progression.

MATERIALS AND METHODS

Strains

All strains were maintained using standard methods (Brenner, 1974). N2 was used as the wild-type strain. Alleles used in this study: *par-1*(*zu310*) (Spilker et al., 2009), *zyg-9*(*b244ts*) (Wood et al., 1980), *par-2*(*it5ts*) (Kirby et al., 1990) and *par-3*(*it71*) (Kirby et al., 1990). Temperature-sensitive

Department of Genetic Medicine and Development, Faculty of Medicine, University of Geneva, 1 rue Michel Servet, 1211 Geneva 4, Switzerland.

*These authors contributed equally to this work
†Author for correspondence (monica.gotta@unige.ch)

Accepted 12 July 2010

strains were grown at 15°C and shifted at semi-permissive or restrictive temperature for 24 hours. PAR-6::HA, GFP::PAR-6, GFP::SPAT-1 and SPAT-1::GFP lines were generated by microparticle bombardment (Praitis et al., 2001) of *unc-119*(*ed3*) mutant worms with *Ppar-6::par-6::HA*, *Ppie-1::gfp::par-6*, *Ppie-1::gfp::spat-1* and *Ppie-1::spat-1::gfp*, respectively, and maintained at 22°C.

RNAi

For *air-1*, dsRNA was produced as described (Zipperlen et al., 2001) using the clone sjj_K07C11.2 (Kamath et al., 2003). *air-1*(*RNAi*) was performed as described (Hannak et al., 2001). Two non-overlapping templates were used for *spat-1*: one covering the first 494 bp and one covering the last 638 bp. Both templates were amplified from *spat-1* cDNA using oligos containing T7 overhangs. dsRNA was transcribed in vitro with T7 polymerase (Promega Ribomax) and injected at a concentration of 0.5-1 mg/ml. As the two dsRNA gave identical results, all experiments were performed using the dsRNA covering the first 494 bp. *spat-1*(*RNAi*) injected worms were kept at 22°C for 22 hours. RNAi of PLK-1 was performed by feeding L4 larvae RNAi bacterial clone sjj_K06H7.1 (Kamath et al., 2003) for 20 hours at 20°C. For co-immunoprecipitation analysis, AIR-1 was depleted by feeding L1 larvae at 20°C.

par-2(*it5ts*) suppression assay

par-2(*it5ts*) L1 larvae were fed with *spat-1*, *par-6* or empty vector containing bacteria and grown at 15°C until L4 larval stage. L4 larvae were shifted to semi-permissive temperature (20°C) and allowed to lay eggs. 24 hours after the temperature shift, the mothers were removed and the plate was kept at 20°C for 24 hours to allow the progeny to hatch. To deplete PLK-1 or AIR-1 in *par-2*(*it5ts*) or wild type, L4 larvae were placed on *plk-1*(*RNAi*) or *air-1*(*RNAi*) bacteria at 20°C for 24 hours and then removed. Viability was assessed by dividing the number of hatched larvae by the total number of progeny (Labbe et al., 2006).

Time-lapse microscopy

Live imaging was conducted using a Leica DM6000 microscope (Leica Microsystems) equipped with epifluorescence and differential interference contrast (DIC) optics. Images were collected every 10 seconds (DIC movies) or 20 seconds (GFP::PAR-6) using a 63×/1.4 NA objective, and the LAS AF software (Leica Microsystems).

Antibody production and immunostaining

A C-terminal fragment of SPAT-1 (amino acid 184 to 545) was cloned into pDEST-MBP (N-terminal Maltose Binding Protein; Gateway). Purified MBP::SPAT-1 was injected into rabbits (Charles River Laboratories). All stainings were performed as described (Spilker et al., 2009). The following primary antibodies were used: anti-tubulin (mouse DM1A, Sigma, 1:1000), anti-SPAT-1 (rabbit, 1:35), anti-PAR-2 (rabbit, 1:50), anti-HA (mouse, 1:200, Sigma) and anti-PLK-1 [rabbit, 1:1000 (Chase et al., 2000)]. Alexa 488 and Alexa 568 secondary antibodies were purchased from Molecular Probes. DNA was revealed with DAPI (Roche). Images were collected using an LSM 510 Meta (Carl Zeiss) confocal microscope with 63×/NA1.4 objective (Carl Zeiss) or Leica DM6000 epifluorescence microscope (Leica Microsystems).

Quantification of fluorescent images

SPAT-1 and PLK-1 cytoplasmic levels were quantified on fixed embryonic samples. Single confocal sections of two- to four-cell embryos stained for SPAT-1 or PLK-1 were taken. Image analysis was performed using ImageJ or LAS AF software (Leica GMBH). Mean cytoplasmic intensities were measured within the regions of interest (ROI). The nuclear and mitotic spindle regions were excluded from the ROI. SPAT-1 levels were normalised to wild-type posterior, whereas PLK-1 levels were normalised to wild-type anterior. The s.e.m. was calculated accordingly. *P*-values were determined by two-tailed *t*-test. The PAR domain length was quantified on wide-field fluorescent images of fixed samples using Leica LAS AF software. PAR-6 normal distribution was considered to spread between 49.5% and 58.5% of embryo length (from the anterior pole). PAR-2 normal distribution was considered to fall between 42.7% and 49.3% of embryo length (from the posterior pole).

Immunoprecipitations

Worms were grown in liquid culture, and embryos were harvested from gravid worms by bleaching (500 mM NaOH, 15% bleach). Embryos were resuspended in IP buffer [100 mM KCl, 50 mM Tris pH 7.5, 1 mM $MgCl_2$, 1 mM DTT, 5% glycerol, 0.05% NP40, 1 mM EDTA, Protease Inhibitor Cocktail (Roche)] and frozen in liquid nitrogen. For protein extraction, the embryos were ground on dry ice using a mortar and pestle. The embryo protein homogenate was thawed on ice and centrifuged at 13,000 rpm for 30 minutes. 450 μg of protein was pre-cleared against 10 μl of Protein A beads for 2 hours at 4°C. The beads were discarded and the extract incubated overnight at 4°C with 10 μg of either PLK-1 or IgG antibody. Next, 15 μl of Protein A beads were added to each tube for 2 hours at 4°C. The beads were washed three times with IP buffer and boiled with SDS sample buffer. The following dilutions of antibodies for western blot were used: PLK-1 1:5000, SPAT-1 1:500 and AIR-1 1:400.

Phosphatase assay

100 μg of embryonic extract, prepared as above, was incubated with 80 units of λ-phosphatase (λ-PPase BioLabs) in the presence or absence of PPase inhibitors [Na_3VO_4 15 mM (Calbiochem), NaF 50 mM, β-glycerophosphate 10 mM and $Na_4O_7P_2$ 10 mM, (Sigma)]. Samples were incubated for 2 hours at 30°C and denatured for 5 minutes at 95°C in SDS sample buffer.

Kinase assay

Kinase assay was performed in kinase buffer [4 mM $MgCl_2$, 10 mM DTT, EDTA-free protease inhibitor (Roche)] in a final volume of 30 μl containing 300 ng of full-length MBP::SPAT-1 or MBP::RHO-1. PLK-1 was immunopurified as described above. 250 ng of *Hs*Plk1 (Cell Signaling Technology) was used per reaction. Reactions were started by adding a mix of 0.6 mM ATP and 5 mCi (γ-^{32}P) ATP (Perkin Elmer). For PLK-1 inhibition, 20 mM of BI2536 (Axon Medchem) was used. Reactions were left for 1 hour at 20°C (PLK-1) or 30 minutes at 30°C (*Hs*Plk-1) and stopped by applying 4×SDS sample buffer. Samples were boiled and loaded on an 8% SDS-PAGE gel. MBP recombinant proteins were visualised by coomassie staining, ^{32}P incorporation was revealed by exposing the gel to an X-ray film.

Yeast two-hybrid analysis

Yeast two-hybrid analysis were performed using a GAL-4 based system (Gateway) in the PJ69-4A yeast strain expressing as bait the full-length PLK-1, the kinase domain or the PBD (C-terminal 309 amino acids of PLK-1) and full-length SPAT-1 as prey. Amino acid substitutions in the PDB domain [as described by Nishi et al. (Nishi et al., 2008)] were inserted by site-directed mutagenesis. Transformed clones hosting the prey-bait positive interaction were selected on selective medium lacking leucine, tryptophan and histidine and containing 3-amino-1,2,4-triazole drug (3AT, Sigma; 25 mM).

RESULTS

SPAT-1/Bora has multiple functions in the early embryo, similar to PLK-1

Whereas human (h) Bora participates in activation of Plk1 (Macurek et al., 2008; Seki et al., 2008b), *Drosophila* Bora promotes Aurora A activation (Hutterer et al., 2006). In *C. elegans*, depletion of the Bora homologue SPAT-1 weakly suppresses *par-2*(*it5ts*) lethality at semi-permissive temperature (Labbe et al., 2006). However, whether SPAT-1 has early embryonic functions is not known. We therefore investigated whether SPAT-1 depletion in otherwise wild-type worms results in embryos with polarity and/or cell division phenotypes.

SPAT-1 depletion by dsRNA injection resulted in embryonic lethality (86%, n>800 embryos), indicating that SPAT-1 has an important role in embryonic development. Longer exposure to RNA interference resulted in sterility of the injected worms. Consistently, homozygous *spat-1* mutants were sterile.

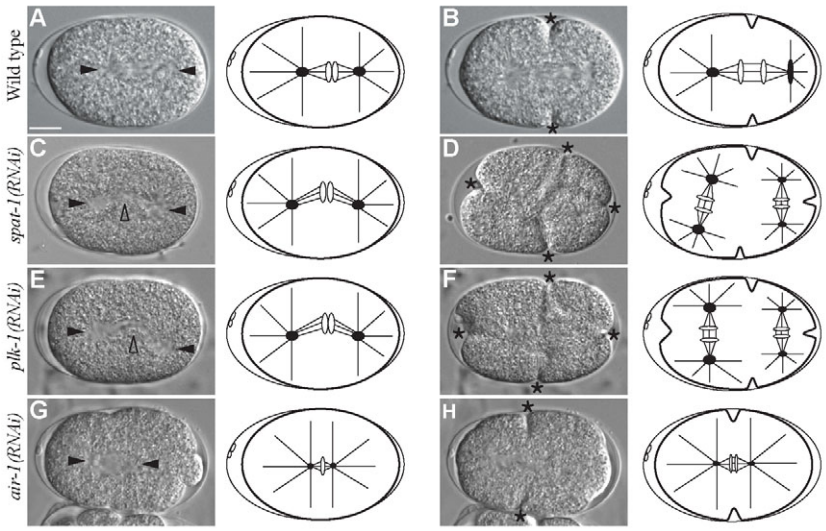

I

	Wild-type	*spat-1(RNAi)*	*plk-1(RNAi)*	*air-1(RNAi)*
Double pseudocleavage	0% (14)	5% (20)	7% (14)	82% (17)
Unstable spindle	0% (20)	51% (45)	31% (16)	0% (19)
Centrosome separation before P0 division	0% (20)	32% (38)	36% (11)	0% (18)
Multiple nuclei	0% (20)	80% (40)	66% (9)	68% (16)
Cytokinesis regression	0% (20)	9% (22)[§]	47% (17)	15% (20)
Pronuclear position at meeting°	68% ± 0.7 (20)	66% ± 1 (19)	65.6% ± 1.4 (12)	52.8% ± 1.4 (19)
Cytokinesis furrow position°	55.2% ± 0.3 (20)	54.7% ± 0.5 (17)	53.5% ± 1 (14)	50.8% ± 1.9 (19)

Fig. 1. *spat-1*(*RNAi*) and *plk-1*(*RNAi*) show similar defects in early *C. elegans* embryos. (**A-H**) Images from time-lapse recordings and respective schematics. In the schemes, black dots represent centrosomes with associated asters (black lines). White ovals represent DNA. (A,C,E,G) The spindle in (C) *spat-1*(*RNAi*) and (E) *plk-1*(*RNAi*) is bent compared with (A) wild type and (G) *air-1*(*RNAi*). The spindle in *air-1*(*RNAi*) (G) is smaller than in wild type (A), as previously reported (Hannak et al., 2001; Schumacher et al., 1998). (B,D,F,H) Centrosome separation in *spat-1*(*RNAi*) (D) and *plk-1*(*RNAi*) (F) occurs before P0 division, leading to a four-way cleavage as compared with the two-way cleavage in wild type (B) and *air-1*(*RNAi*) (H). Solid arrowheads indicate centrosomes; open arrowheads the spindle mid-zone. Asterisks indicate cytokinesis furrows. (**I**) Quantification of phenotypes. Pronuclear position at meeting and cytokinesis furrow position were calculated as a percentage of egg length ° ±s.e.m., with 0 and 100% representing anterior and posterior ends, respectively. [§]For cytokinesis regression, embryos in which centrosome separation was impaired were not taken into consideration. The number of embryos analysed is shown in parentheses. In this and subsequent figures, anterior is to the left, posterior to the right. Scale bar: 10 μm.

We analysed the first two cell divisions of *spat-1*(*RNAi*) embryos using time-lapse microscopy. In wild type, sperm entry triggers the completion of meiosis and defines the posterior pole of the one-cell embryo (P0). The maternal pronucleus migrates towards the posterior to meet the paternal pronucleus. Meanwhile, cortical contractions contribute to the formation of the PAR domains. Contractions culminate in the pseudocleavage, a deep invagination of the cortex that corresponds to the border between anterior and posterior PAR domains. After meeting, the pronuclear-centrosomal complex undergoes a 90° rotation while moving to the centre of the embryo. The mitotic spindle forms in the centre of the embryo and aligns along the A-P axis. At metaphase the spindle is displaced towards the posterior, resulting in an asymmetric first division with a bigger anterior cell (AB), and a smaller posterior cell (P1). AB and P1 differ in size, fate and cell-cycle timing (Gonczy and Rose, 2005) (see Movie 1 in the supplementary material).

spat-1(*RNAi*) embryos had a complex phenotype showing several abnormalities. Meiosis was impaired, as indicated by the presence of several female pronuclei and abnormally large polar bodies (data not shown). The P0 mitotic spindle was unstable, either moving back and forth along the A-P axis or with both poles displaying exaggerated transverse oscillation and spindle bending in the middle (Fig. 1C,I; see Movie 2 in the supplementary material). The cleavage furrow regressed in 9% of embryos (Fig. 1I). In 32% of one-cell embryos, centrosomes separated before P0 cytokinesis had occurred and three or more furrows ingressed simultaneously, resulting in a three- or four-cell embryo (Fig. 1D,I; see Movie 2 in the supplementary material). DNA segregation was aberrant, as indicated by the presence of multiple nuclei (Fig. 1I) and lagging chromosomes (see Fig. S2 in the supplementary material). Cell cycle progression was delayed in all cells (described below).

spat-1(*RNAi*) embryos resembled *plk-1*(*RNAi*) embryos. The mitotic spindle in *plk-1*(*RNAi*) embryos was unstable (Fig. 1E,I), whereas it collapsed in *air-1*(*RNAi*) embryos (Fig. 1G) (Hannak et al., 2001; Schumacher et al., 1998). Centrosomes separated before P0 cytokinesis in *plk-1*(*RNAi*) embryos but not in *air-1*(*RNAi*) embryos (Fig. 1F,H,I). In addition, although depletion of AIR-1 often resulted in the formation of two pseudocleavages, this occurred rarely in *plk-1*(*RNAi*) and *spat-1*(*RNAi*) embryos (Fig. 1I).

Our results indicate that SPAT-1 regulates several processes in the early embryo, including spindle stability, DNA segregation and cell cycle progression. Furthermore, we found that the phenotypes resulting from SPAT-1 depletion were similar to the phenotypes resulting from PLK-1 depletion, suggesting that SPAT-1/Bora works with PLK-1 in regulating cell division processes in *C. elegans* embryos.

SPAT-1 depletion, like PLK-1 depletion, delays cell cycle progression

Aurora A and Polo kinases are crucial for mitotic entry (Archambault and Glover, 2009; Meraldi et al., 2004). In the *C. elegans* embryo, AIR-1 localises to centrosomes (Hannak et al., 2001; Schumacher et al., 1998) and promotes timely mitotic entry and nuclear envelope breakdown (NEBD) in one-cell embryos (Hachet et al., 2007; Portier et al., 2007). Enrichment of PLK-1 in AB in two-cell embryos promotes earlier mitotic entry of AB with

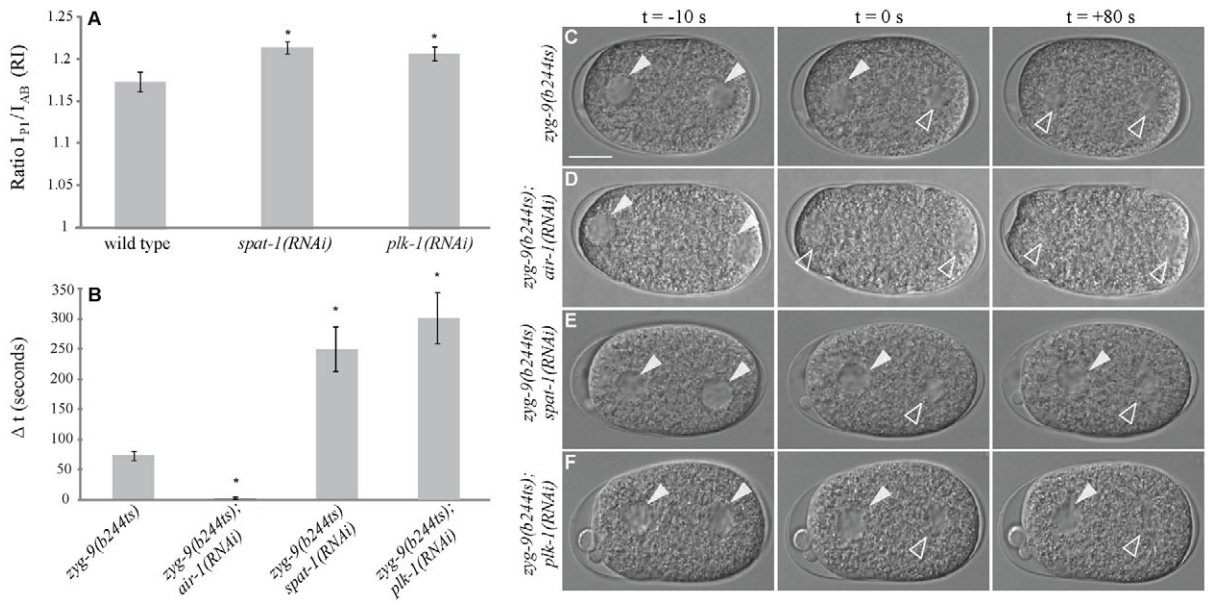

Fig. 2. Depletion of SPAT-1 and PLK-1 results in cell cycle delay. (**A**) Mean values ± s.e.m. of the ratio of duration of interphase (RI) between P1 (I_{P1}) and AB (I_{AB}) in wild-type, *spat-1*(*RNAi*) and *plk-1*(*RNAi*) *C. elegans* embryos. **P*<0.05. Numerical values and two-tailed *t*-test results are shown in Table S1 in the supplementary material. (**B**) The interval (Δt; mean values in seconds ± s.e.m.) between NEBD of male and female pronucleus in one-cell embryos. **P*<0.01. For corresponding values and two-tailed *t*-test, see Table S2 in the supplementary material. (**C-F**) DIC images of one-cell embryos undergoing mitosis. Left column, embryos 10 seconds before male pronucleus NEBD; middle column, embryos at male pronucleus NEBD (*t*=0 seconds); right column, embryos 80 seconds after male pronucleus NEBD. Solid arrowheads indicate pronuclei with an intact nuclear envelope; open arrowheads indicate the position of the pronuclei at or after NEBD. Scale bar: 10 μm.

respect to P1 (Budirahardja and Gonczy, 2008; Rivers et al., 2008). Depletion of PLK-1 results in a cell cycle delay in AB but a more extensive delay in P1. The ratio of duration of interphase (RI) in P1 over AB is higher in PLK-1-depleted embryos than in wild type (Fig. 2A) (Budirahardja and Gonczy, 2008; Rivers et al., 2008). We found that *spat-1*(*RNAi*) embryos had a significant cell cycle delay in P0, AB and P1 (see Table S1 in the supplementary material and data not shown). As in PLK-1-depleted embryos, the RI was higher in *spat-1*(*RNAi*) embryos compared with wild type (Fig. 2A and see Table S1 in the supplementary material). By contrast, *air-1*(*RNAi*) embryos had a variable phenotype, with 50% of embryos in which both AB and P1 was delayed (RI higher than the wild type), 21% of embryos in which AB and P1 divided synchronously (RI=1), 21% of embryos in which P1 divided before AB (RI<1) and 8% of embryos behaving like wild type (*n*=14). Such variability was not observed in *plk-1*(*RNAi*) and *spat-1*(*RNAi*) embryos.

To further investigate whether AIR-1, PLK-1 and SPAT-1 play similar and/or distinct roles in cell cycle progression, we took advantage of an assay designed to monitor the timing of mitotic entry (Hachet et al., 2007). In wild-type embryos, the maternal and paternal pronuclei meet in the posterior and move to the centre, where they undergo almost simultaneous NEBD (Portier et al., 2007). In mutants in which the migration of the female pronucleus is defective, such as *zyg-9* mutants (Matthews et al., 1998), the two pronuclei remain apart and enter mitosis asynchronously, as scored by following NEBD. The male pronucleus, which is associated with the centrosomes, enters mitosis with normal timing, whereas the female pronucleus is delayed by about 80 seconds (delay hereafter referred to as 'Δt'). The centrosomes serve as centres for the recruitment of AIR-1, which, in the *zyg-9* mutant, drives entry into mitosis of the male pronucleus with normal timing (Hachet et al., 2007). Consistently, in double *zyg-9*(*b244ts*)*;air-1*(*RNAi*) embryos, although the two pronuclei remained apart, they entered mitosis simultaneously but both were delayed (Fig. 2B,D and see Table S2 in the supplementary material).

We investigated the phenotype of PLK-1 and SPAT-1 depletion in *zyg-9*(*b244ts*). The separated pronuclei undergo asynchronous NEBD in *zyg-9*(*b244ts*) (Δt ≈ 80s, Fig. 2B,C) and this asynchrony is abolished upon *air-1*(*RNAi*) (Fig. 2B,D) (Hachet et al., 2007). Conversely, *spat-1*(*RNAi*) or *plk-1*(*RNAi*) in *zyg-9*(*b244ts*) resulted in increased asynchrony (Fig. 2B,E,F), with the female pronucleus undergoing NEBD in average 250 and 300 seconds, respectively, after the male pronucleus. The increased asynchrony was not due to premature NEBD of the male pronucleus, as this was delayed in *plk-1*(*RNAi*) and *spat-1*(*RNAi*), as in *air-1*(*RNAi*) embryos (see Table S2 in the supplementary material) (Hachet et al., 2007).

Our data indicate that SPAT-1 and PLK-1, like AIR-1, are required for timely mitotic entry, as male NEBD was delayed in their absence. However, SPAT-1 and PLK-1 play an additional role in mitotic entry, as the delay of female NEBD was increased in double *zyg-9*(*b244ts*)*;plk-1*(*RNAi*) and *zyg-9*(*b244ts*) *spat-1*(*RNAi*) embryos.

SPAT-1 and PLK-1 interact in an AIR-1-independent manner

Our data point to a model in which SPAT-1 works with PLK-1 in regulating early embryonic processes and mitotic entry. We tested whether these two proteins interact. We observed an interaction between SPAT-1 and a fragment of PLK-1 containing the polo-box domain (PBD) (Fig. 3A,B) by yeast two-hybrid. We could not detect an interaction using the kinase domain of PLK-1 nor full-length PLK-1.

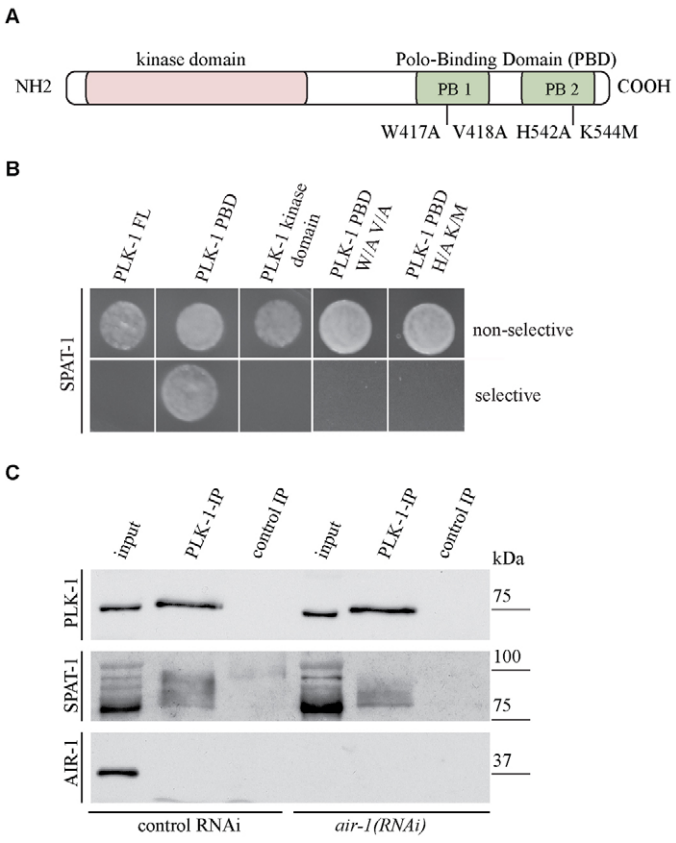

Fig. 3. SPAT-1 interacts with PLK-1. (**A**) Schematic of PLK-1. The kinase domain and polo-box domain (PBD) with the two polo boxes (PB1 and PB2) indicated. The key residues for PBD phosphopeptide binding and their substitutions are marked. (**B**) PLK-1-PBD interacts with SPAT-1 in a yeast two-hybrid assay. Bait plasmids express full-length (FL) PBD, kinase domain and PBD mutated forms of PLK-1. Each colony tested contained the prey plasmid expressing SPAT-1 and a bait plasmid expressing the proteins indicated. Yeast hosting positive interaction between bait and prey proteins grow on selective medium (bottom row). (**C**) Co-immunoprecipitation from wild-type and *air-1*(*RNAi*) *C. elegans* embryos using PLK-1 antibodies. Western blots were probed with antibodies to SPAT-1, PLK-1 or AIR-1 as indicated on the left. As both SPAT-1 and PLK-1 migrate around 75 kDa, two independent gels were run and blotted. Input:IP=1:15.

The PBD targets PLK-1 to phosphorylated substrates to allow proper mitotic progression (Elia et al., 2003; Seong et al., 2002). Several residues in the PBD of human Plk1 are crucial for phosphopeptide binding (Elia et al., 2003). In *C. elegans* PLK-1, substitution of tryptophan 417 and valine 418 for alanine in the first polo box and of histidine 542 and lysine 544 for alanine and methionine, respectively, in the second polo box (Fig. 3A) abolishes binding to MEX-5 (Nishi et al., 2008). The same substitutions abolished binding of PLK-1 to SPAT-1 (Fig. 3B), suggesting that the interaction between PLK-1-PBD and SPAT-1 in yeast requires initial SPAT-1 phosphorylation.

We next tested whether PLK-1 and SPAT-1 interact in vivo. We raised an antibody to SPAT-1 that recognised several bands with different mobility at about 80 kDa in western blots of embryonic extracts (see Fig. S1A in the supplementary material). These bands were lost upon depletion of SPAT-1, indicating that they are specific. Upon treatment with λ-phosphatase, the SPAT-1 signal was reduced to one band (see Fig. S1B in the supplementary material), indicating that SPAT-1 is modified by phosphorylation at multiple sites in vivo. We immunoprecipitated PLK-1 from embryonic extracts and successfully co-immunoprecipitated SPAT-1 (Fig. 3C). Consistent with the two-hybrid analysis, PLK-1 mostly precipitated the phosphorylated forms of SPAT-1 (Fig. 3C). AIR-1 was not detected in the co-immunoprecipitate. Furthermore, SPAT-1 and PLK-1 co-immunoprecipitated in extract depleted of AIR-1, indicating that the interaction of PLK-1 with SPAT-1 is AIR-1 independent.

Therefore, PLK-1 and SPAT-1, consistent with their similar roles in regulating cell division processes, can form a complex in vivo.

PLK-1 and SPAT-1 depletion suppress *par-2*(*it5ts*) lethality and restore PAR-2 posterior cortical localisation

Depletion of SPAT-1 and PLK-1 results in very similar cell division phenotypes, and these two proteins form a complex in vivo. We therefore tested whether PLK-1 depletion, like SPAT-1 depletion, could rescue the lethality of *par-2*(*it5ts*) (Labbe et al., 2006).

Whereas *par-2*(*it5ts*) show a viability of about 5% (Fig. 4A) at semi-permissive temperature, SPAT-1 or PAR-6 depletion in *par-2*(*it5ts*) results in a reproducible and significant increase in viability (Fig. 4A) (Labbe et al., 2006; Watts et al., 1996). Partial depletion of PLK-1 was also able to restore *par-2*(*it5ts*) viability to a similar extent as *spat-1*(*RNAi*) (Fig. 4A), despite the fact that *plk-1*(*RNAi*) in the same conditions in wild type resulted in low viability (Fig. 4B). By contrast, AIR-1 depletion could not rescue *par-2*(*it5ts*) lethality. Instead embryonic lethality increased to 100%, most likely the consequence of an additive effect (Fig. 4A).

We next addressed how SPAT-1 and PLK-1 depletion could suppress *par-2*(*it5ts*) lethality by following the localisation of PAR-2 on fixed embryos. In one-cell wild-type embryos, PAR-2 was enriched at the posterior cortex (Fig. 4C). By contrast, PAR-2 was hardly detectable at the cortex in 90% of *par-2*(*it5ts*) embryos (Fig. 4D, *n*=37). Consistent with the partial suppression of *par-2*(*it5ts*) lethality, *par-6*(*RNAi*) restored a weak PAR-2 cortical localisation at the posterior in 50% of embryos, (Fig. 4H, *n*=43). RNAi of *spat-1* (*n*=67) and *plk-1* (*n*=84) in *par-2*(*it5ts*) also restored the posterior cortical PAR-2 localisation in 42% and 39% of embryos, respectively (Fig. 4E,F). Double *par-2*(*it5ts*)*plk-1*(*RNAi*) and *spat-1*(*RNAi*);*par-2*(*it5ts*) embryos displayed abnormal DNA segregation and cytokinesis defects (data not shown), as did the single *plk-1*(*RNAi*) and *spat-1*(*RNAi*) embryos (our unpublished data) (Chase et al., 2000), which could account for the mild lethality suppression seen in double mutants compared with the high rescue of cortical PAR-2 in these embryos. PAR-2 posterior cortical localisation was not restored upon depletion of AIR-1 in *par-2*(*it5ts*) (Fig. 4G, 0%, *n*=31), consistent with the lack of suppression.

Our data show that PLK-1 depletion, like SPAT-1 depletion, results in suppression of *par-2*(*it5ts*) lethality and restores PAR-2 cortical localisation, suggesting that the two proteins work together in polarity regulation.

SPAT-1 and PLK-1 have a similar role in polarity

We next investigated whether PLK-1 and SPAT-1 play a role in regulating the localisation of PAR proteins in wild-type embryos. We analysed the localisation of PAR-2 and PAR-6 in one-cell embryos at the pronuclear meeting stage or later. At this time point in wild type, polarity establishment has occurred and PAR-2 is restricted to the posterior and PAR-6 to the anterior pole (Fig. 5A)

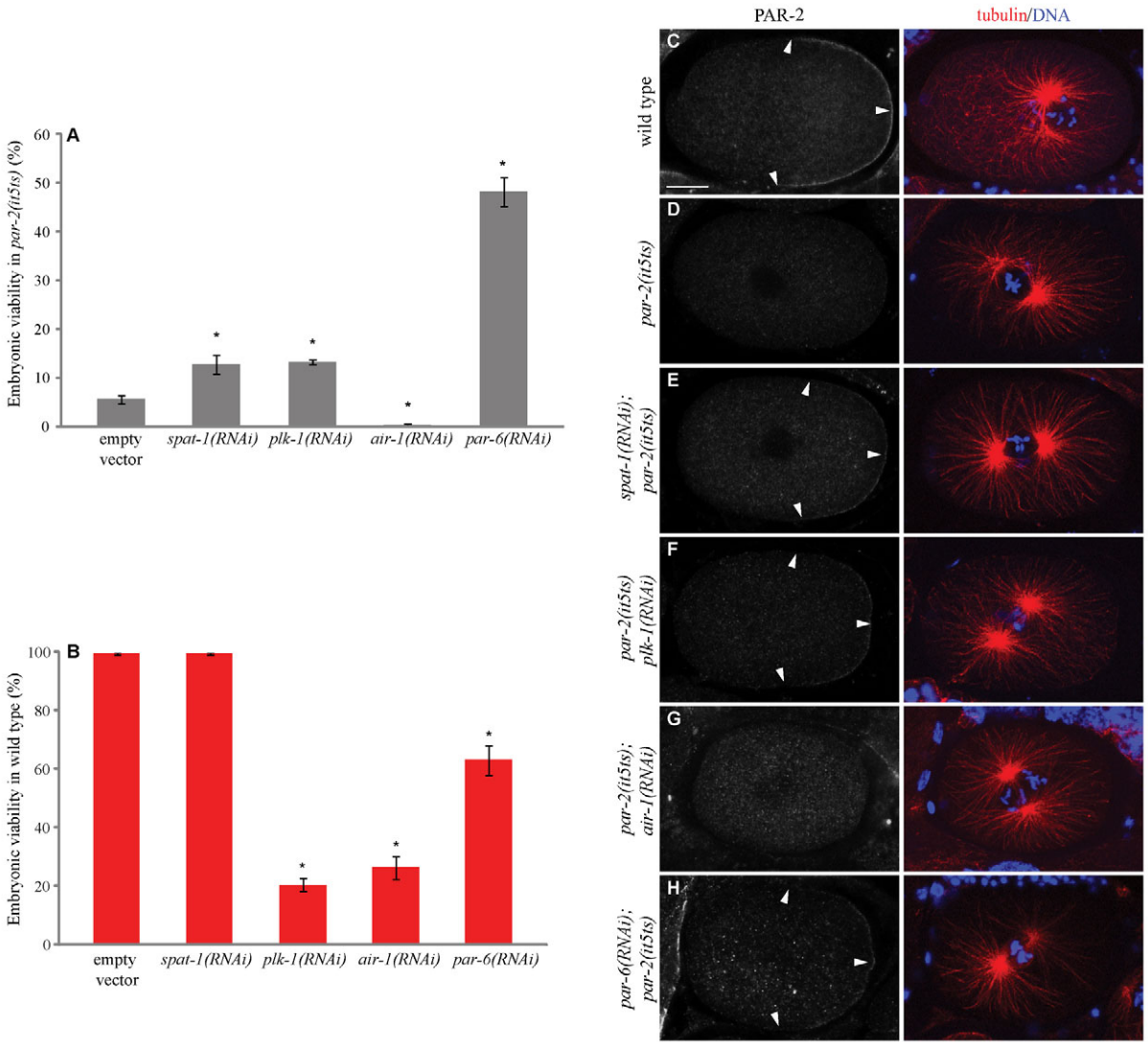

Fig. 4. SPAT-1 and PLK-1 depletion suppresses *par-2(it5ts)* lethality. (**A**,**B**) Embryonic viability of *par-2*(*it5ts*) (A) or wild-type *C. elegans* embryos (B) upon depletion of the indicated proteins. The values correspond to the percentage of embryos that hatched over the total number of embryos ± s.e.m. Embryonic viability was assessed by counting more than 400 progeny for each genotype. Three independent experiments were performed. **P*<0.05. (**C-H**) Distribution of PAR-2 in one-cell-stage embryos. Arrowheads indicate cortically localised PAR-2. Corresponding merged images of tubulin (red) and DNA (blue) are displayed in the right-hand column. Scale bar: 10 μm.

(Cuenca et al., 2003). Anterior and posterior domains are mutually exclusive, with PAR-6 occupying about 54% of embryo length. In both *spat-1*(*RNAi*) and *plk-1*(*RNAi*) embryos, PAR-6 and PAR-2 occupied distinct domains, mostly anterior for PAR-6 and posterior for PAR-2, indicating that establishment of an A-P axis occurs and mutual exclusion of PAR proteins is functional. However, the respective expansion and the precise localisation of the PAR domains were aberrant. In the majority of *spat-1*(*RNAi*) embryos, PAR domain expansion along the A-P axis varied or the border between the anterior and posterior PAR domains was not perpendicular with respect to the A-P axis (hereafter defined as shifted domains; Fig. 5B,E). In 5% of embryos we observed PAR-2 localisation at both poles, with PAR-6 being restricted to a central band (Fig. 5E). The remaining embryos appeared as wild type. Similarly to SPAT-1-depleted embryos, the majority of *plk-1*(*RNAi*) embryos displayed a PAR domain abnormally expanded or shifted along the A-P axis (Fig. 5C,E), 8% had a PAR-2 domain at both poles and the remaining embryos appeared as wild type (Fig. 5E). By contrast, 49% of *air-1*(*RNAi*) embryos displayed a strong loss of polarity, with PAR-2 present at both poles and PAR-6 restricted in the centre (Fig. 5D,E). This is consistent with data showing that P granules, a polarity marker restricted to the posterior in wild type, are localised at both poles in *air-1*(*RNAi*) embryos (Schumacher et al., 1998). Abnormal domain expansion or shifted domains were observed in 32% of embryos, and the remaining 19% had no apparent defects (Fig. 5E).

To further characterise the PAR polarity phenotype, we monitored cell polarisation in vivo using a GFP::PAR-6 strain. In wild type GFP::PAR-6 is initially found all around the cortex. This symmetry is broken before pronuclear migration by the male centrosomes and associated microtubules (reviewed by Munro and Bowerman, 2009). GFP::PAR-6 follows cortical contractions to the anterior pole clearing the posterior. By pronuclear meeting GFP::PAR-6 occupies 48±3.1% of the embryonic cortex (*n*=23)

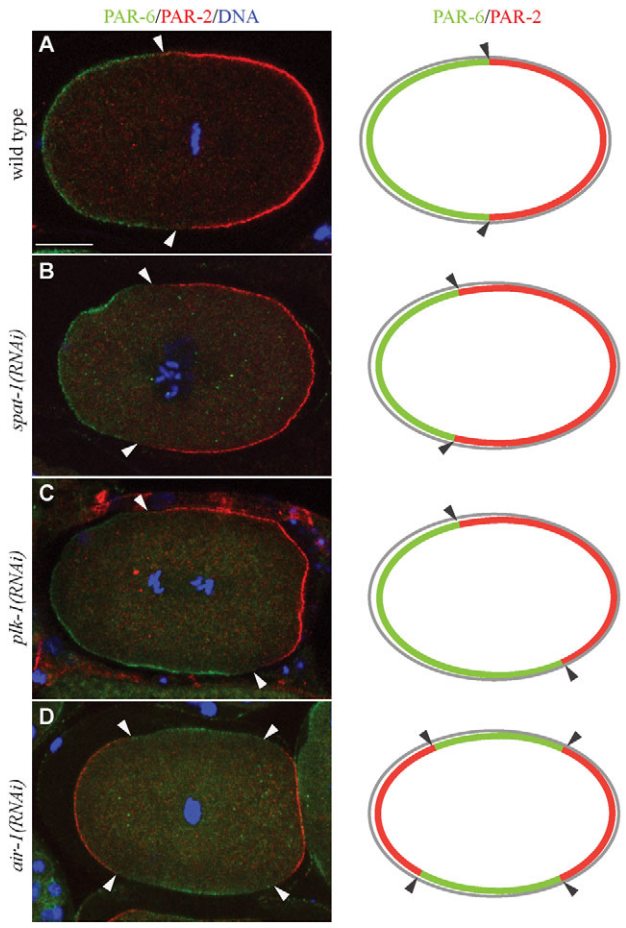

E PAR protein localisation classes

genotype	a	b + c	d
wild type (25)	84 %	16 % *	0 %
spat-1(RNAi) (54)	28 %	67 %	5 %
plk-1(RNAi) (48)	29 %	63 %	8 %
air-1(RNAi) (43)	19 %	32 %	49 %

Fig. 5. SPAT-1 and PLK-1 play a similar role in polarity. (**A-D**) (Left) Localisation of PAR-6 (green), PAR-2 (red) and DNA (blue). (Right) Schematic of PAR protein localisation. (A) PAR-6 is at the anterior cortex and PAR-2 at the posterior cortex in wild type. (B) An example in which PAR domains vary in expansion along the A-P axis. (C) An example in which the border between the anterior and posterior PAR domains is not perpendicular with respect to the A-P axis (shifted). (D) An example in which PAR-2 is localised at both poles, whereas PAR-6 is restricted to a central band. Arrowheads point at the border between PAR-6 and PAR-2 domains. (**E**) Quantification of phenotypes shown in A-D. (*) Shifted PAR domains were never observed in wild type. The number of embryos analysed is shown in parentheses. Scale bar: 10 μm.

(see Movie 3 in the supplementary material). Upon SPAT-1 (n=19) or PLK-1 (n=14) depletion, GFP::PAR-6 cleared the posterior as in wild type. However, at pronuclear meeting *spat-1*(*RNAi*) and *plk-1*(*RNAi*) embryos displayed a shorter PAR-6 domain compared with wild type in 84% and 72% of embryos, respectively [see Movie 4 in the supplementary material, *spat-1*(*RNAi*)]. In two *spat-1*(*RNAi*) and two *plk-1*(*RNAi*) embryos, the PAR-6 domain shifted along the A-P axis [see Movie 5 in the supplementary material, *plk-1*(*RNAi*)]. In all cases the polarity boundary was corrected at division, as described (Schenk et al., 2010).

Altogether, depletion of PLK-1 and SPAT-1 results in similar defects in the distribution of PAR proteins in one-cell embryos that are different from the most representative polarity defect of *air-1*(*RNAi*) embryos.

SPAT-1 is enriched in posterior cells

We subsequently addressed SPAT-1 localisation in early embryos. Using antibodies against SPAT-1, we found that SPAT-1 was cytoplasmic but was also found in the nucleus and around kinetochores. In four-cell embryos SPAT-1 levels were higher in the two posterior cells, EMS and P2 (see Fig. S1C in the supplementary material). This enrichment became detectable in late two-cell stage embryos (Fig. 6A,K and see Table S3 in the supplementary material). The cytoplasmic and nuclear staining pattern are specific, as they were lost in *spat-1*(*RNAi*) embryos (see Fig. S1C in the supplementary material). The staining around kinetochores was highly reduced but not lost upon SPAT-1 depletion, suggesting that we are unable to fully deplete SPAT-1 or that the residual staining is unspecific.

To study the dynamics of SPAT-1 localisation, we constructed transgenic lines expressing GFP::SPAT-1 or SPAT-1::GFP. Both fusions resulted in the same localisation pattern. Consistent with the antibody-staining pattern, SPAT-1 was a cytoplasmic protein. Some fraction of SPAT-1 entered the pronuclei during centration (see Fig. S1D in the supplementary material) and is again released into the cytoplasm upon NEBD. During metaphase SPAT-1 became enriched around kinetochores (see Fig. S1D in the supplementary material). However, neither GFP::SPAT-1 nor SPAT-1::GFP were enriched in posterior cells. This could be due to overexpression of the transgene or partial disruption of its function by the GFP moiety.

In conclusion, SPAT-1 localises in the cytoplasm, in the nucleus and around kinetochores. Furthermore, cytoplasmic SPAT-1 is enriched in posterior cells.

SPAT-1 enrichment depends on polarity cues and PLK-1

We next investigated how mutations in the *par* genes influence SPAT-1 distribution. In both *par-1* and *par-3* mutants the asymmetric distribution of SPAT-1 was lost. In *par-1*(*zu310*) and *par-2*(*RNAi*) embryos SPAT-1 levels were equal in AB and P1 and as low as in AB in wild type (Fig. 6B,K and see Table S3 in the supplementary material; data not shown). In *par-3*(*it71*) SPAT-1 levels were also symmetric but high in both AB and P1 as in P1 in wild type (Fig. 6C,K and see Table S3 in the supplementary material). Therefore, both the asymmetry and the cytoplasmic levels of SPAT-1 depend on PAR proteins.

In the *C. elegans* embryo the localisation of PLK-1 is complementary to the localisation of SPAT-1. PLK-1 is enriched in the anterior cell AB whereas SPAT-1 was enriched in the posterior cell P1 (Fig. 6F and 6A, respectively). Furthermore, SPAT-1 and PLK-1 levels are controlled in a reciprocal way by PAR proteins. In *par-1*(*zu310*) embryos, SPAT-1 levels were low whereas PLK-1 levels were high in all cells (Fig. 6B,G,K,L) (Budirahardja and Gonczy, 2008; Rivers et al., 2008). In *par-3*(*it71*) embryos SPAT-1 levels were high in all cells whereas PLK-1 levels are low (Fig. 6C,H,K,L) (Budirahardja and Gonczy, 2008; Rivers et al., 2008). We therefore investigated whether the asymmetric distribution and levels of SPAT-1 are

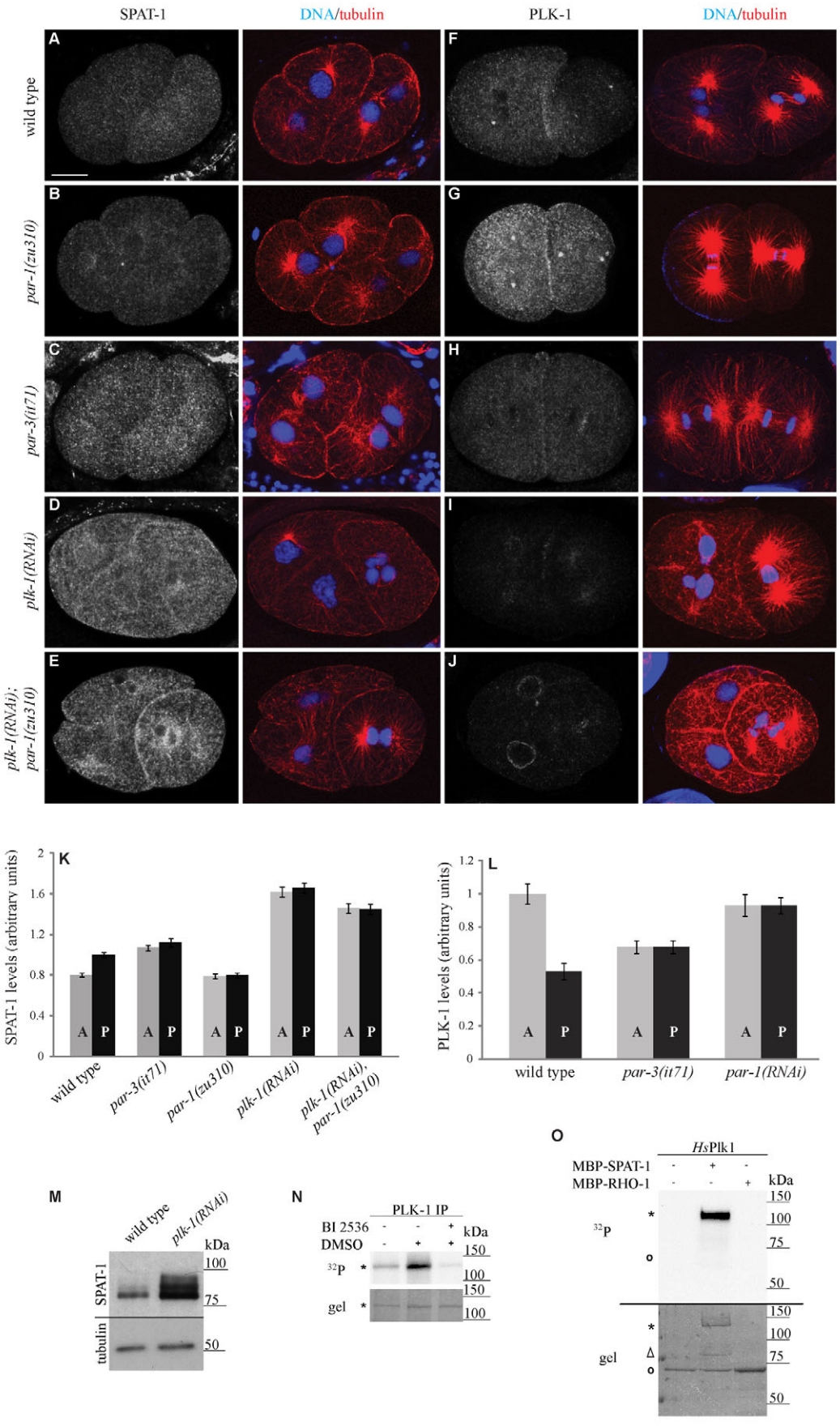

Fig. 6. SPAT-1 enrichment depends on PAR proteins and PLK-1. (**A-J**) Localisation of SPAT-1 (A-E) and PLK-1 (F-J) in late two-cell-stage *C. elegans* embryos. Corresponding merged images of tubulin (red) and DNA (blue) are also shown. (**K**,**L**) Normalised fluorescent cytoplasmic intensities of SPAT-1 (K) and PLK-1 (L) in anterior and posterior cells. At least ten embryos were measured for each genotype. Mean values ± s.e.m. are shown. For corresponding *P*-values, see Table S3 in the supplementary material. (**M**) Embryonic extracts of wild-type and PLK-1-depleted embryos probed for SPAT-1 or tubulin. (**N**,**O**) PLK-1 phosphorylates SPAT-1. Kinase assays conducted using the indicated substrates and PLK-1 immunoprecipitated from *C. elegans* (N) or human (O) Plk1. Upper panels show ^{32}P incorporation visualised by autoradiography, whereas lower panels show coomassie-stained gels. In N, phosphorylation of MBP::SPAT-1 was tested in the absence or presence of the Plk1 inhibitor BI2536. Phosphorylation is greatly diminished upon addition of BI 2536. In O, MBP::RHO-1 is used as negative control. Asterisks indicate MBP-SPAT; the open circle marks MBP-RHO-1, which co-migrates with human (*Hs*) Plk1 in O, as detected by a more intense coomassie staining. A, anterior; P, posterior. Scale bar: 10 μm.

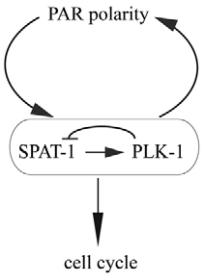

Fig. 7. Working model for SPAT-1 and PLK-1 in coupling PAR polarity and cell cycle. Lines with bars show antagonistic interactions, whereas lines with arrows depict positive interactions. In this model, SPAT-1 positively regulates the activity of PLK-1, whereas PLK-1 negatively regulates SPAT-1. The SPAT-1–PLK-1 complex is regulated by PAR polarity and regulates PAR polarity. PLK-1 and SPAT-1 also regulate the cell cycle, providing a link between cell polarity and cell cycle progression during asymmetric cell division.

regulated by PLK-1. We found that in *plk-1*(*RNAi*) embryos SPAT-1 levels were strongly increased and equal in all cells (Fig. 6D,K,M). Conversely, PLK-1 localisation was not affected in *spat-1*(*RNAi*) early embryos (see Fig. S2 in the supplementary material). These data show that SPAT-1 levels are regulated by PLK-1. In human cells, Plk1 phosphorylates Bora and targets it for degradation (Chan et al., 2008; Seki et al., 2008a). Consistent with this, we found that PLK-1 immunoprecipitated from embryos as well as human Plk1 phosphorylated bacterially expressed SPAT-1, suggesting that, like in human cells, SPAT-1 is phosphorylated by PLK-1 and targeted to degradation (Fig. 6N,O).

PAR-1 negatively regulates PLK-1 (Budirahardja and Gonczy, 2008; Rivers et al., 2008), and we have shown that PLK-1 negatively regulates SPAT-1 levels. If the low SPAT-1 levels in *par-1* mutants depend on PLK-1, SPAT-1 levels should again increase in *plk-1*(*RNAi*);*par-1*(*zu310*) embryos. Indeed, SPAT-1 levels are elevated in *plk-1*(*RNAi*);*par-1*(*zu310*) embryos, resembling *plk-1*(*RNAi*) embryos alone (Fig. 6E,K). Therefore PLK-1 is epistatic to PAR-1 in the regulation of SPAT-1 levels.

In conclusion, we find that SPAT-1 levels and localisation are under the control of PAR polarity and PLK-1 (Fig. 7).

DISCUSSION

Our findings show that SPAT-1 and PLK-1 control polarity and cell cycle progression, two processes that are tightly regulated during asymmetric cell division. Whereas PAR polarity regulates the localisation of both SPAT-1 and PLK-1 (this work) (Budirahardja and Gonczy, 2008; Rivers et al., 2008), both PLK-1 and SPAT-1 are required for proper PAR protein localisation and timely mitotic entry, providing a link between cell polarity and cell cycle progression (Fig. 7).

Whereas in asymmetrically dividing *Drosophila* cells Bora regulates Aurora A activity (Hutterer et al., 2006), in symmetrically dividing mammalian cells Bora is essential to regulate Plk1 activity for G2 to M transition (Chan et al., 2008; Seki et al., 2008a; Seki et al., 2008b). hBora binds to Plk1 and makes it accessible to be phosphorylated by Aurora A, which results in activation of Plk1. Our genetic, phenotypic and biochemical data suggest a model in which SPAT-1 activates PLK-1 and not AIR-1 in asymmetrically dividing *C. elegans* embryos. We have shown that SPAT-1 and PLK-1 form a complex in vivo in an AIR-1-independent manner. The phenotypes resulting from SPAT-1 depletion in wild type or mutants are similar to the phenotypes observed upon depletion of PLK-1 and often distinct from the phenotypes resulting from AIR-1 depletion. The similarity of phenotypes between SPAT-1- and PLK-1-depleted embryos, the fact that SPAT-1 and PLK-1 interact, and the mammalian data showing that hBora is required for the activity of Plk1 suggest that SPAT-1 also acts on PLK-1 activity in *C. elegans*. Consistent with this model, the localisation of PLK-1 was not affected upon SPAT-1 depletion. Our data cannot exclude the possibility that AIR-1 activates PLK-1 in *C. elegans*. However, if AIR-1 was activating PLK-1, upon *air-1*(*RNAi*) PLK-1 would be inactive, which in turn would lead to accumulation of SPAT-1, as observed in *plk-1*(*RNAi*) embryos. Yet we did not see such an increase in SPAT-1 levels in *air-1*(*RNAi*) embryos (data not shown). Either AIR-1 is not needed for PLK-1 activation in *C. elegans*, or AIR-1 works redundantly with another kinase. Indeed, hBora is required for PLK1 activation by Aurora A for G2 to mitosis transition (Seki et al., 2008b). However, Plk1 is also active in mitosis despite the fact that hBora is degraded (Chan et al., 2008; Seki et al., 2008a). This indicates that either Aurora A uses another co-factor to activate Plk1 or that another kinase is required for Plk1 activation during mitosis progression (Macurek et al., 2009).

SPAT-1 enrichment in posterior cells is clearly detectable starting from late two-cell embryos, whereas PLK-1 anterior enrichment has already started in one-cell embryos. Either SPAT-1 regulation by PLK-1 is not active in early embryos, or such regulation exists but is weak and cannot be detected by staining. If SPAT-1 is required for PLK-1 activity, why are SPAT-1 levels low in anterior cells, where PLK-1 is more active? This pattern might be the consequence of feedback regulation by PLK-1, which, once activated by SPAT-1, downregulates SPAT-1 levels to inhibit its own further activation, as in mammalian cells. A second possibility is that SPAT-1 can be both an activator and an inhibitor of PLK-1, depending on its levels. Whereas low levels of SPAT-1 would promote PLK-1 activity in the anterior cells, high levels could inhibit PLK-1 in posterior cells. An example of a factor behaving both as an activator and inhibitor is not uncommon. For instance, securin has a dual function on separase. It promotes separase accumulation in the nucleus, but it also acts as a separase inhibitor and must therefore be degraded in anaphase (Hornig et al., 2002). As SPAT-1 levels are increased upon PLK-1 depletion, we favour the first model. Therefore, our data indicate that SPAT-1 and PLK-1 work together in regulating polarity and cell cycle progression and suggest that SPAT-1 is required to regulate PLK-1 activity.

How could PLK-1 and SPAT-1 regulate PAR polarity? Similar to the reduction of levels or activity of components of the anterior PAR complex, depletion of PLK-1 can suppress *par-2*(*it5ts*). The activity of the anterior complex might be reduced upon PLK-1 depletion. An alternative possibility is that PAR-2 activity in *par-2*(*it5ts*) is partially restored when PLK-1 is depleted. A plausible possibility is that PAR proteins are substrates of PLK-1 phosphorylation. PLK-1 putative phosphorylation sites exist in all anterior PAR proteins and in PAR-2. PLK-1 may phosphorylate one of the anterior PAR proteins and activate the anterior complex. PLK-1 depletion would result in reduced activity of the anterior complex and rescue of *par-2*(*it5ts*) lethality. Conversely, PLK-1 may be a negative regulator of PAR-2. Partial depletion of PLK-1 in *par-2*(*it5ts*), where PAR-2 is compromised, could restore some PAR-

2 activity and suppress the lethality. Both possibilities are in agreement with the defect in PAR domain expansion that we observed when PLK-1 or SPAT-1 were depleted in an otherwise wild-type background. Another possibility is that PLK-1 acts on other substrates that can modulate the activity of PAR proteins. A known substrate of PLK-1 in *C. elegans* is the CCCH containing protein MEX-5 (Nishi et al., 2008). Phosphorylation of MEX-5 by PLK-1 enhances the activity of MEX-5. However, it is unlikely that MEX-5 is the PLK-1 substrate involved in PAR polarity regulation, because *mex-5* mutants have polarity defects that are different from the defects in PAR protein localisation observed upon depletion of PLK-1 (Cuenca et al., 2003; Schubert et al., 2000). Furthermore, depletion of *mex-5* does not result in *par-2* lethality rescue (our unpublished results). Finally, PLK-1 may regulate the cytoskeletal machinery that localise PAR proteins in one-cell embryos.

PLK-1 and SPAT-1 depletion, like AIR-1 depletion, results in mitotic entry delay. However, SPAT-1 and PLK-1 have additional functions that are distinct from AIR-1 in cell cycle progression. Whereas AIR-1 depletion abolished the interval between male and female NEBD in a *zyg-9* mutant, PLK-1 or SPAT-1 depletion dramatically increased this delay. AIR-1 localises at centrosomes and promotes timely mitotic entry. However, as entry into mitosis occurs in the absence of AIR-1, another pathway may help trigger mitosis in these embryos (Hachet et al., 2007). We propose that SPAT-1 and PLK-1 are components of this alternative pathway. Our data also suggest that cytoplasmic (versus centrosomal) PLK-1 can be active in promoting mitotic entry, as NEBD of the female pronucleus, which does not have centrosomes but is surrounded by cytoplasmic PLK-1, is delayed in absence of PLK-1.

In some *spat-1*(*RNAi*) and *plk-1*(*RNAi*) one-cell embryos, duplicated centrosomes separated before completion of cytokinesis, which resulted in ingression of multiple furrows. This is not merely a consequence of a cell cycle delay of these embryos, as other mutants that are also delayed do not display such phenotype (our unpublished data). It rather indicates that SPAT-1 and PLK-1 are also required for the coordination between the centrosomal cycle and cell cycle.

Taken together, our data show that in *C. elegans* SPAT-1/Bora works with PLK-1 in regulating mitotic entry and PAR polarity and provides a molecular link for the coordination of cell polarity and cell cycle during asymmetric cell division.

Acknowledgements

We thank S. Boulton, A. Golden, Y. Kohara, S. Paulillo, D. Rivers and E. Zanin for reagents; R. Loewith for help with the kinase assay; P. Meraldi, L. Pintard, M. Prouteau, M. Sohrmann and F. Spiga for comments on the manuscript; and members of the M.G. laboratory and Patrick Meraldi for discussions and advice. Some strains used in this work were provided by the National BioResource Project (NBRP)::*C. elegans* and by the *Caenorhabditis* Genetics Center (funded by the NIH National Center of Research Resources). This work was supported by a grant from the Swiss National Science Foundation to M.G. and by funding from the University of Geneva.

Competing interests statement

The authors declare no competing financial interests.

Supplementary material

Supplementary material for this article is available at
http://dev.biologists.org/lookup/suppl/doi:10.1242/dev.055293/-/DC1

References

Archambault, V. and Glover, D. M. (2009). Polo-like kinases: conservation and divergence in their functions and regulation. *Nat. Rev. Mol. Cell Biol.* **10**, 265-275.

Boyd, L., Guo, S., Levitan, D., Stinchcomb, D. T. and Kemphues, K. J. (1996). PAR-2 is asymmetrically distributed and promotes association of P granules and PAR-1 with the cortex in C. elegans embryos. *Development* **122**, 3075-3084.

Brenner, S. (1974). The genetics of Caenorhabditis elegans. *Genetics* **77**, 71-94.

Budirahardja, Y. and Gonczy, P. (2008). PLK-1 asymmetry contributes to asynchronous cell division of C. elegans embryos. *Development* **135**, 1303-1313.

Chan, E. H., Santamaria, A., Sillje, H. H. and Nigg, E. A. (2008). Plk1 regulates mitotic Aurora A function through betaTrCP-dependent degradation of hBora. *Chromosoma* **117**, 457-469.

Chase, D., Serafinas, C., Ashcroft, N., Kosinski, M., Longo, D., Ferris, D. K. and Golden, A. (2000). The polo-like kinase PLK-1 is required for nuclear envelope breakdown and the completion of meiosis in Caenorhabditis elegans. *Genesis* **26**, 26-41.

Cuenca, A. A., Schetter, A., Aceto, D., Kemphues, K. and Seydoux, G. (2003). Polarization of the C. elegans zygote proceeds via distinct establishment and maintenance phases. *Development* **130**, 1255-1265.

Elia, A. E., Rellos, P., Haire, L. F., Chao, J. W., Ivins, F. J., Hoepker, K., Mohammad, D., Cantley, L. C., Smerdon, S. J. and Yaffe, M. B. (2003). The molecular basis for phosphodependent substrate targeting and regulation of Plks by the Polo-box domain. *Cell* **115**, 83-95.

Etemad-Moghadam, B., Guo, S. and Kemphues, K. J. (1995). Asymmetrically distributed PAR-3 protein contributes to cell polarity and spindle alignment in early C. elegans embryos. *Cell* **83**, 743-752.

Gonczy, P. (2008). Mechanisms of asymmetric cell division: flies and worms pave the way. *Nat. Rev. Mol. Cell Biol.* **9**, 355-366.

Gonczy, P. and Rose, L. S. (2005). Asymmetric cell division and axis formation in the embryo. *WormBook*, 1-20. www.wormbook.org.

Guo, S. and Kemphues, K. J. (1995). par-1, a gene required for establishing polarity in C. elegans embryos, encodes a putative Ser/Thr kinase that is asymmetrically distributed. *Cell* **81**, 611-620.

Hachet, V., Canard, C. and Gonczy, P. (2007). Centrosomes promote timely mitotic entry in C. elegans embryos. *Dev. Cell* **12**, 531-541.

Hannak, E., Kirkham, M., Hyman, A. A. and Oegema, K. (2001). Aurora-A kinase is required for centrosome maturation in Caenorhabditis elegans. *J. Cell Biol.* **155**, 1109-1116.

Hao, Y., Boyd, L. and Seydoux, G. (2006). Stabilization of cell polarity by the C. elegans RING protein PAR-2. *Dev. Cell* **10**, 199-208.

Hornig, N. C., Knowles, P. P., McDonald, N. Q. and Uhlmann, F. (2002). The dual mechanism of separase regulation by securin. *Curr. Biol.* **12**, 973-982.

Hung, T. J. and Kemphues, K. J. (1999). PAR-6 is a conserved PDZ domain-containing protein that colocalizes with PAR-3 in Caenorhabditis elegans embryos. *Development* **126**, 127-135.

Hutterer, A., Berdnik, D., Wirtz-Peitz, F., Zigman, M., Schleiffer, A. and Knoblich, J. A. (2006). Mitotic activation of the kinase Aurora-A requires its binding partner Bora. *Dev. Cell* **11**, 147-157.

Kamath, R. S., Fraser, A. G., Dong, Y., Poulin, G., Durbin, R., Gotta, M., Kanapin, A., Le Bot, N., Moreno, S., Sohrmann, M. et al. (2003). Systematic functional analysis of the Caenorhabditis elegans genome using RNAi. *Nature* **421**, 231-237.

Kirby, C., Kusch, M. and Kemphues, K. (1990). Mutations in the par genes of Caenorhabditis elegans affect cytoplasmic reorganization during the first cell cycle. *Dev. Biol.* **142**, 203-215.

Labbe, J. C., Pacquelet, A., Marty, T. and Gotta, M. (2006). A genomewide screen for suppressors of par-2 uncovers potential regulators of PAR protein-dependent cell polarity in Caenorhabditis elegans. *Genetics* **174**, 285-295.

Li, J., Kim, H., Aceto, D. G., Hung, J., Aono, S., Kemphues, K. J. (2010). Binding to PKC-3, but not to PAR-3 or to a conventional PDZ domain ligand, is required for PAR-6 function in C. elegans. *Dev. Biol.* **340**, 88-98.

Macurek, L., Lindqvist, A., Lim, D., Lampson, M. A., Klompmaker, R., Freire, R., Clouin, C., Taylor, S. S., Yaffe, M. B. and Medema, R. H. (2008). Polo-like kinase-1 is activated by aurora A to promote checkpoint recovery. *Nature* **455**, 119-123.

Macurek, L., Lindqvist, A. and Medema, R. H. (2009). Aurora-A and hBora join the game of Polo. *Cancer Res.* **69**, 4555-4558.

Matthews, L. R., Carter, P., Thierry-Mieg, D. and Kemphues, K. (1998). ZYG-9, a Caenorhabditis elegans protein required for microtubule organization and function, is a component of meiotic and mitotic spindle poles. *J. Cell Biol.* **141**, 1159-1168.

Meraldi, P., Honda, R. and Nigg, E. A. (2004). Aurora kinases link chromosome segregation and cell division to cancer susceptibility. *Curr. Opin. Genet. Dev.* **14**, 29-36.

Munro, E. and Bowerman, B. (2009). Cellular symmetry breaking during Caenorhabditis elegans development. *Cold Spring Harbor Perspect. Biol.* **1**, a003400.

Nishi, Y., Rogers, E., Robertson, S. M. and Lin, R. (2008). Polo kinases regulate C. elegans embryonic polarity via binding to DYRK2-primed MEX-5 and MEX-6. *Development* **135**, 687-697.

Portier, N., Audhya, A., Maddox, P. S., Green, R. A., Dammermann, A., Desai, A. and Oegema, K. (2007). A microtubule-independent role for centrosomes and aurora a in nuclear envelope breakdown. *Dev. Cell* **12**, 515-529.

Praitis, V., Casey, E., Collar, D. and Austin, J. (2001). Creation of low-copy integrated transgenic lines in Caenorhabditis elegans. *Genetics* **157**, 1217-1226.
Rivers, D. M., Moreno, S., Abraham, M. and Ahringer, J. (2008). PAR proteins direct asymmetry of the cell cycle regulators Polo-like kinase and Cdc25. *J. Cell Biol.* **180**, 877-885.
Schenk, C., Bringmann, H., Hyman, A. A. and Cowan, C. R. (2010). Cortical domain correction repositions the polarity boundary to match the cytokinesis furrow in C. elegans embryos. *Development* **137**, 1743-1753.
Schubert, C. M., Lin, R., de Vries, C. J., Plasterk, R. H. and Priess, J. R. (2000). MEX-5 and MEX-6 function to establish soma/germline asymmetry in early C. elegans embryos. *Mol. Cell* **5**, 671-682.
Schumacher, J. M., Ashcroft, N., Donovan, P. J. and Golden, A. (1998). A highly conserved centrosomal kinase, AIR-1, is required for accurate cell cycle progression and segregation of developmental factors in Caenorhabditis elegans embryos. *Development* **125**, 4391-4402.
Seki, A., Coppinger, J. A., Du, H., Jang, C. Y., Yates, J. R., 3rd and Fang, G. (2008a). Plk1- and beta-TrCP-dependent degradation of Bora controls mitotic progression. *J. Cell Biol.* **181**, 65-78.
Seki, A., Coppinger, J. A., Jang, C. Y., Yates, J. R. and Fang, G. (2008b). Bora and the kinase Aurora a cooperatively activate the kinase Plk1 and control mitotic entry. *Science* **320**, 1655-1658.
Seong, Y. S., Kamijo, K., Lee, J. S., Fernandez, E., Kuriyama, R., Miki, T. and Lee, K. S. (2002). A spindle checkpoint arrest and a cytokinesis failure by the dominant-negative polo-box domain of Plk1 in U-2 OS cells. *J. Biol. Chem.* **277**, 32282-32293.
Spilker, A. C., Rabilotta, A., Zbinden, C., Labbe, J. C. and Gotta, M. (2009). MAP kinase signaling antagonizes PAR-1 function during polarization of the early Caenorhabditis elegans embryo. *Genetics* **183**, 965-977.
Tabuse, Y., Izumi, Y., Piano, F., Kemphues, K. J., Miwa, J. and Ohno, S. (1998). Atypical protein kinase C cooperates with PAR-3 to establish embryonic polarity in Caenorhabditis elegans. *Development* **125**, 3607-3614.
Watts, J. L., Etemad-Moghadam, B., Guo, S., Boyd, L., Draper, B. W., Mello, C. C., Priess, J. R. and Kemphues, K. J. (1996). par-6, a gene involved in the establishment of asymmetry in early C. elegans embryos, mediates the asymmetric localization of PAR-3. *Development* **122**, 3133-3140.
Wood, W. B., Hecht, R., Carr, S., Vanderslice, R., Wolf, N. and Hirsh, D. (1980). Parental effects and phenotypic characterization of mutations that affect early development in Caenorhabditis elegans. *Dev. Biol.* **74**, 446-469.
Zipperlen, P., Fraser, A. G., Kamath, R. S., Martinez-Campos, M. and Ahringer, J. (2001). Roles for 147 embryonic lethal genes on C.elegans chromosome I identified by RNA interference and video microscopy. *EMBO J.* **20**, 3984-3992.

Table S1. Mean cell cycle timing (in seconds ± s.e.m.) of the interphase of AB (l_{AB}) and P1 cell (l_{P1}) scored as an interval between NEBD of AB cell and P0 and NEBD of P1 cell and P0, respectively

	Δt (seconds)				*P*-values		
Genotype	l_{P0}–l_{AB}	l_{P0}–l_{P1}	Ratio l_{P1}/l_{AB}	*n*	l_{P0}–l_{AB}	l_{P0}–l_{P1}	Ratio l_{P1}/l_{AB}
Wild type	751±15	891±15	1.19±0.01	7	–	–	–
control(RNAi)	827±31	987±40	1.19±0.01	7	0.025	0.026	0.75
spat-1(RNAi)	901±30	1108±35	1.23±0.01	15	<0.001	<0.001	0.002
plk-1(RNAi)	897±65	1103±78	1.22±0.01	7	0.09	0.058	0.027

Data are plotted in Fig. 2A. Genotypes of analysed worms are indicated. *n* corresponds to the number of embryos analysed. *P*-values were calculated by two-tailed *t*-test comparing mutants with wild type.

Table S2. Mean time (in seconds ± s.e.m.) separating meiosis II exit from NEBD of the male and female pronuclei and the interval between female and male NEBD in embryos of the indicated genotypes

Genotype	Meiosis II exit – male NEBD	Meiosis II exit – female NEBD	Δt (seconds)	*n*	*P*-value
zyg-9(b244ts)	555±12	630±14	73±8	9	–
air-1(RNAi);zyg-9(b244ts)	788±42	791±42	2.5±3	8	<0.001
spat-1(RNAi)zyg9(b244ts)	675±50	925±77	250±37	6	<0.001
plk-1(RNAi);zyg-9(b244ts)	866±55	1173±91	301±42	6	0.003

Data are represented in Fig. 2B. The number of embryos analysed (*n*) and *P*-values [calculated for Δt by two-tailed *t*-test comparing double mutants with the single *zyg-9(b244ts)*] are indicated.

Table S3. Normalised cytoplasmic SPAT-1 levels in embryos of the indicated genotypes

	Normalised cytoplasmic SPAT-1 levels		*P*-values			
			Wild-type anterior		Wild-type posterior	
Genotype	Anterior	Posterior	Anterior	Posterior	Anterior	Posterior
Wild type	0.79±0.03	1.00±0.02	–	<0.01	<0.01	–
par-3(it71)	1.07±.0.03	1.12±0.04	<0.01	<0.01	0.2	0.058
par-1(zu310)	0.79±0.03	0.80±0.03	0.86	0.52	<0.01	<0.01
plk-1(RNAi)	1.62±0.05	1.66±0.05	<0.01	<0.01	<0.01	<0.01
plk-1(RNAi);par-1(zu310)	1.46±0.05	1.46±0.05	<0.01	<0.01	<0.01	<0.01

Values represent mean fluorescence intensities of cytoplasmic SPAT-1 ± s.e.m. for data plotted in Fig. 6K. Values were normalised according to SPAT-1 levels in the wild-type posterior cell. Two-tailed *t*-test was used to compare the mutant with the control anterior and posterior values.